

## Transactions of The Indian Institute of Metals

Vol. 64, Issues 1 & 2, February-April 2011, pp. 71-74

# Fracture toughness of $t'$ $\text{ZrO}_2$ stabilised with $\text{MO}_{1.5}$ ( $\text{M} = \text{Y}, \text{Yb} \& \text{Gd}$ ) for thermal barrier application

**Archana Loganathan and Ashutosh S. Gandhi**

*Department of Metallurgical and Materials Engineering*

*Indian Institute of Technology Madras*

*Chennai – 600036*

*E-mail: archanalog@gmail.com*

*Received 04 November 2010*

*Revised 23 February 2011*

*Accepted 25 February 2011*

*Online at www.springerlink.com*

*© 2011 TIIM, India*

**Keywords:**

*thermal barrier coatings; fracture toughness; rare-earth stabilisers; spark plasma sintering*

### **Abstract**

Thermal Barrier coatings (TBC's) protect the gas turbine blades at high temperature exposure. The  $t'$  phase is metastable and slowly transforms to the high-temperature equilibrium state consisting of tetragonal ( $t$ ) and cubic ( $c$ ) during high temperature exposure. A comparative study of the phase stability and fracture toughness of monolithic Y, Yb and Gd stabilised zirconia with composition 8 mol% $\text{MO}_{1.5}$  was studied. Powders were prepared by co-precipitation method with crystallite size ~15 nm. Pressureless sintering, Spark plasma sintering (SPS) at 1250°C for 10 min was carried out to produce compacts with >96% relative density for fracture toughness measurements XRD and Raman studies revealed the initial phase was  $t'$ . After sintering, no spontaneous monoclinic phase formed during cooling. The fracture toughness of the sintered pellets of different composition was measured. The results were analysed in terms of the effect of phase constitution on fracture toughness. The role of ferroelastic toughening in these materials was explored.

### **1. Introduction**

Thermal barrier coatings (TBC's) protect the superalloy components in a gas turbine engine at higher temperatures and increase the durability of these components. Engine efficiency can also be increased by using TBC's [1]. The typical TBC system comprises of (1) the substrate, usually nickel base superalloy; (ii) the metallic bond coat (BC); (iii) the ceramic top coat (TBC), and (iv) thermally grown oxide (TGO) scale that forms on the bond coat during service, as the top coat is not impervious to oxygen [1,2]. The prime requirements for TBC material selection are low thermal conductivity, low density, phase stability, high melting point, low thermal expansion mismatch with the underlying superalloy and good adherence. Moreover, the TBC should not react with the TGO, i.e. be thermochemically compatible with it [1-5]. Ceramic top coats are deposited using either air plasma spraying (APS) or electron beam physical-vapor deposition (EB-PVD) [1, 5, 6]. At present the most successful TBC material is 6-8 wt% of  $\text{YO}_{1.5}$  in  $\text{ZrO}_2$ , yttria stabilized zirconia (YSZ) [3]. The initial phase in these YSZ compositions is the  $t'$  tetragonal zirconia. This metastable phase does not transform to monoclinic zirconia even in the presence of large stresses. Hence  $t'$  zirconia does not exhibit transformation toughening [1, 5, 7-9]. However, at the TBC service temperature of ~1150°C, the  $t'$  phase is prone to slowly transform into a two-phase ( $t + c$ ) structure. This occurs by the precipitation of the cubic phase and concurrent depletion of yttria from the tetragonal phase.

Different types of failure occur in the thermal barrier coating system. Considering the case of delamination of top coat, this is caused by stresses developed during thermal cycling (intrinsic failure) or penetration of molten salts or

erosion or foreign object damage (extrinsic failures). In the intrinsic failure modes, the stresses increase as the temperature of the system decreases. The crack initiates at the TGO/TBC interface and propagates through the TBC near this interface. Hence, the inherent room temperature fracture toughness of the TBC material is the focus of this paper [2, 5, 12-14]. The  $t'$  YSZ has higher fracture toughness when compared with cubic YSZ and the newer 'low- $k$ ' TBC materials which contain up to four stabilisers [10]. Moreover, the thermal conductivity of Y-TZP is higher than  $t'$  and cubic phases. The development of higher fracture toughness for TBC materials has been one of the important recent issues in the area of TBC's.

The  $t'$  phase does not exhibit transformation toughening and its higher toughness has been ascribed to ferroelastic toughening [17, 18]. Ferroelastic domain nucleation as well as domain switching are believed to be responsible for toughening. However, the mechanisms and microstructural aspects of toughening in zirconia based TBC materials have not been understood so far. It must be noted that the widely known transformation toughening due to tetragonal to monoclinic transformation ( $t \rightarrow m$ ) [15, 16] is seen in YSZ with lower yttria content than TBC's (6 wt%  $\text{YO}_{1.5}$ , e.g. Y-TZP). Moreover, transformation toughening is restricted to low temperatures. As the temperature increases (>900°C), the transformation toughening gradually decreases and disappears [15].

In the present study, the fracture toughness at room temperature for the as-sintered pellets of 8 mol%  $\text{MO}_{1.5}$  stabilized zirconia ( $\text{M} = \text{Y}, \text{Yb}$  and  $\text{Gd}$ ) has been studied. It is known that lanthanide series stabilisers impart lower thermal conductivity to zirconia. The effect of these stabilisers on the inherent fracture toughness of  $t'$  zirconia

has not been reported so far. Processing of coatings of various compositions is time consuming. Moreover, TBC material fracture toughness measurement is not straightforward. Hence, dense monolithic materials of the above mentioned compositions were prepared and their indentation fracture toughness was studied.

## 2. Experimental details

Nanocrystalline powders of  $\text{ZrO}_2$ -8 mol%  $\text{MO}_{1.5}$  ( $\text{M} = \text{Y}$ ,  $\text{Yb}$  and  $\text{Gd}$ ) were prepared by reverse co-precipitation method. The compositions are designated as YSZ, YbSZ and GdSZ, respectively. Nitrate of  $\text{Y}$ ,  $\text{Yb}$  or  $\text{Gd}$  (99.9% pure, Alfa Aesar) and zirconium oxynitrate (99.9% purity, Sigma Aldrich) were dissolved in de-ionized water to 0.3 M concentration. The mixed nitrate solution was added drop-wise to a  $\text{NH}_4\text{OH}$  solution with pH maintained at 9. Poly-ethylene glycol (PEG) was added as a surfactant in the ammonia solution for minimising the agglomeration during synthesis. The mixed hydroxide precipitate was washed repeatedly with de-ionized water and ethanol before drying at 120°C for 5h. The powders were calcined at 700°C for 2 h, then ball milled for breaking down the agglomerates for 4 h at 250 rpm using in a planetary ball mill (Fritsch Pulverisette 6). Tungsten carbide vial and balls, and terpineol as wet milling medium were used.

The YSZ powders were densified by pressureless sintering, while YbSZ and GdSZ were densified by spark plasma sintering (SPS). For conventional sintering, the ball milled powders of YSZ were cold uniaxially pressed at a high pressure of 850 MPa to further break down agglomerates and achieve high green density. The green compact was sintered at 1250°C for 2 h in a muffle furnace (OKAY, 70F 4). Ball milled powders of YbSZ and GdSZ were densified using SPS (Dr. Sinter, 625), in vacuum using cylindrical graphite die of 12 mm diameter. Densification was carried at 1250°C for 10 min at the heating rate of >150°C/min, with a current of 1000 A and uniaxial pressure of 50 MPa. The density was measured by Archimedes' method.

Fracture toughness of the dense pellets was measured by indentation technique after ceramographic polishing. Vickers hardness tester (Wolpert Wilson 4325VA) with a load of 3kg for 10 sec was used for indentation. The toughness was measured as the energy release rate  $\Gamma$  by:

$$\Gamma = \frac{K_c^2}{E} = 2\zeta^2 P \left( \frac{d^2}{c^3} \right) \quad (1)$$

where  $\Gamma$  is the toughness in  $\text{Jm}^{-2}$ ,  $K_c$  is the fracture toughness ( $\text{MPa}\sqrt{\text{m}}$ ),  $E$  is Young's modulus,  $\zeta$  is a geometry factor ( $\approx 0.016$ ),  $P$  is the load (N),  $d$  is the size of the indentation, and  $c$  is length of a crack emanating from a corner of the indentation [11, 19]. Using Scanning electron microscopy (SEM, FEI Quanta 200),  $d$  and  $c$  are measured. The toughness is reported as the average of values obtained from 4-6 indentations.

The phase constitution of the calcined, ball milled powder and pellets were analysed using X-ray diffraction (XRD) with  $\text{Cu}-\text{K}\alpha$  radiation (Bruker AXS D8). XRD scanning were collected in steps of 0.02°, with 1's dwell time, in the diffraction angle range of 25°-38°, and 0.01° with 4's dwell time in the range of 71°-76°. The crystallite size  $d$  was calculated using Scherrer formula.

$$d = \frac{0.9\lambda}{B \cos\theta} \quad (2)$$

Here,  $\lambda$  is X-ray wavelength,  $B$  the peak width corrected for instrumental broadening, and  $\theta$  the Bragg angle. The instrumental broadening was estimated using  $\alpha$ -alumina powder annealed at 1500°C for 2 h. For the sintered pellets, the 004<sub>t</sub> and 400<sub>t</sub> peak data from slow scans before indentation were used for calculating c/a ratio of the tetragonal phase.

Raman spectra were obtained for calcined, ball milled and sintered pellets using Horiba Jobin Yvov HR 800 UV Raman spectrometer equipped with a thermoelectrically cooled CCD. The Raman spectra of 100-800  $\text{cm}^{-1}$  were measured using an He-Ne laser of source 632.8 nm. Phase change in the case of calcined, ball milled and sintered pellets have been studied from spectrum obtained.

## 3. Results and discussion

The XRD studies from the three compositions was investigated in all the three stages of preparation (as-synthesised, ball milled and sintered pellets). The XRD patterns in the 2θ range between 25° to 38° and 72° to 76° from the sintered pellets is shown in Fig. 1. All the samples were tetragonal and there was no trace of either the monoclinic or the cubic zirconia phases [20]. Raman spectroscopy confirmed the tetragonal nature for all the composition [21, 22] and also in the case of sintered pellets, the patterns exhibit the (002)/(200) split as shown in Fig.1(a). The crystallite size estimated from the width of the (004)<sub>t</sub>/(400)<sub>t</sub> peaks is shown in Fig.2. The initial crystallite size of as-synthesised powders was less than ~15 nm and there was an increase in crystallite size after sintering. The final crystallite sizes of GdSZ was the smallest in this set (44 nm), whereas the YbSZ had the largest crystallite size of 61 nm. The tetragonality (c/a) calculated from the (004)<sub>t</sub> and (400)<sub>t</sub> peaks (Table-I) increased in the sequence YbSZ, YSZ and GdSZ. This is commensurate with the ionic radii of the three stabilisers [23].

Raman spectra for all the three conditions were recorded. Raman spectroscopy is highly sensitive to the presence of monoclinic phase. Figure 3 shows the Raman spectra from the densified compacts. There was no indication of the monoclinic phase in any of the three compositions. After calcinations and sintering, the six bands present in the Raman spectra confirmed the t' phase [21].

The sintered densities in the present study were greater than ~96%. The fracture toughness values measured on YSZ, YbSZ and GdSZ are listed in Table 1, along with values for c/a calculated from XRD. The toughness values are higher for the three compositions when compared with the literature values reported for t' YSZ (~45  $\text{Jm}^{-2}$ ) [11]. Typical indentation for the YSZ is shown in Fig.4. The GdSZ has the highest fracture toughness of 117  $\text{Jm}^{-2}$  in this study, while YSZ and YbSZ have similar toughness. The GdSZ specimen had a significantly higher tetragonality and smaller crystallite size. Raman spectroscopy was carried out at the crack tip in YSZ, where the probe diameter was ~1 mm. There was no monoclinic phase present at the crack tip (not shown here), which was confirmed by the absence of Raman bands from monoclinic phase at 182 and 191  $\text{cm}^{-1}$  [21, 24]. The role of transformation toughening in t' YSZ in this study can be ruled out. One of the significant factors for the increase in toughness of all the samples when compared to literature

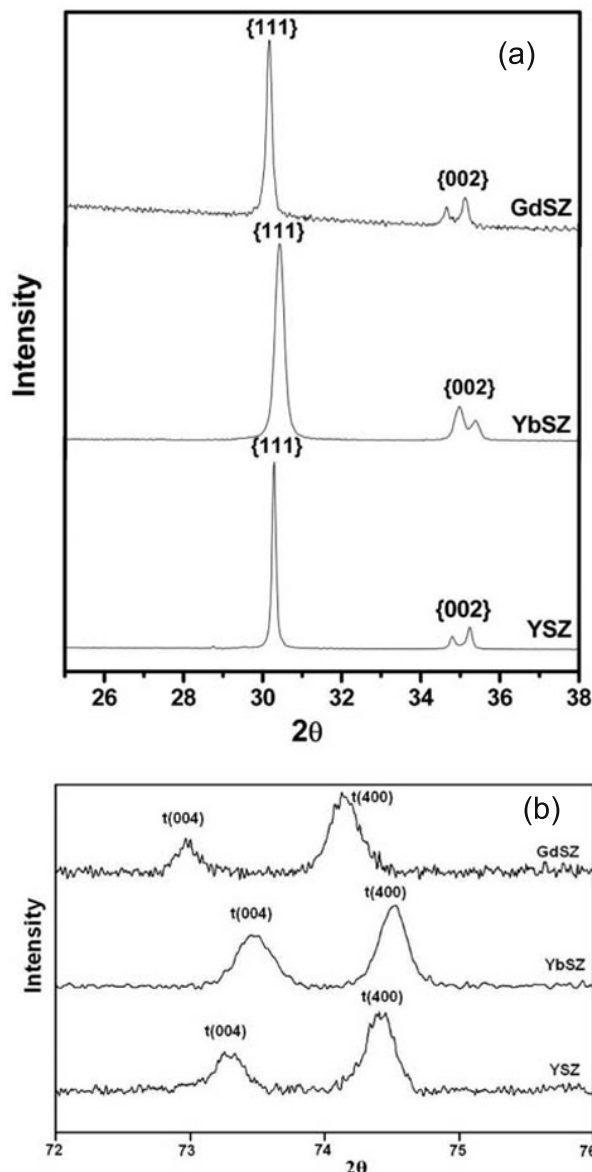


Fig. 1 : XRD patterns of the three compositions of the as-densified pellets. YSZ was pressureless sintered, YbSZ and GdSZ were spark plasma sintered. (a) Diffraction angle range of  $25^\circ$ - $38^\circ$ , (b) diffraction angle range of  $72^\circ$ - $76^\circ$ .

values of  $t'$  YSZ is the nanocrystalline crystallite size obtained after sintering. In nanocrystalline ceramics, the critical flaw is much larger than the grain/crystallite size [25]. Therefore, the crystallite size is expected to influence only the toughening mechanism that is present in the material. In the absence of transformation toughening the  $t'$  phases are likely to exhibit ferroelastic toughening. Both, domain nucleation and switching can occur in the process zone

Table 1 : Fracture toughness ( $Jm^{-2}$ ) and tetragonality of as-densified YSZ, YbSZ and GdSZ materials.

Composition	Type of Sintering	Fracture toughness $\Gamma$ ( $Jm^{-2}$ )	$c/a$
YSZ	Pressureless sintering	$90 \pm 5$	1.0131
YbSZ	SPS	$87 \pm 8$	1.0117
GdSZ	SPS	$117 \pm 8$	1.0142

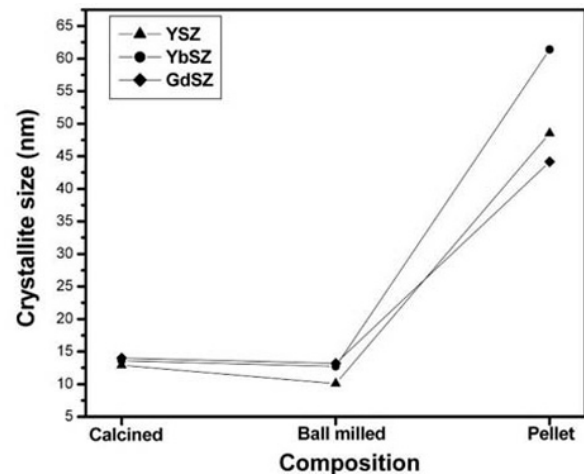


Fig. 2 : Average crystallite size calculated from XRD.

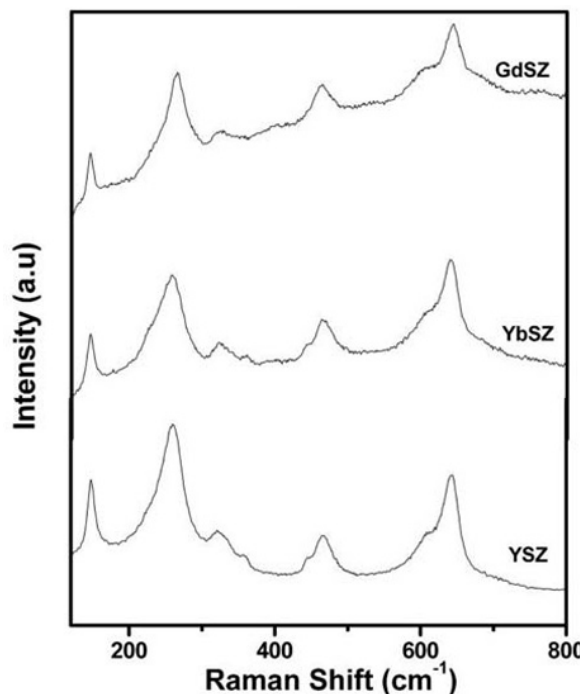


Fig. 3 : Raman spectrum obtained from the as-densified pellets indicating the presence of tetragonal phase only.

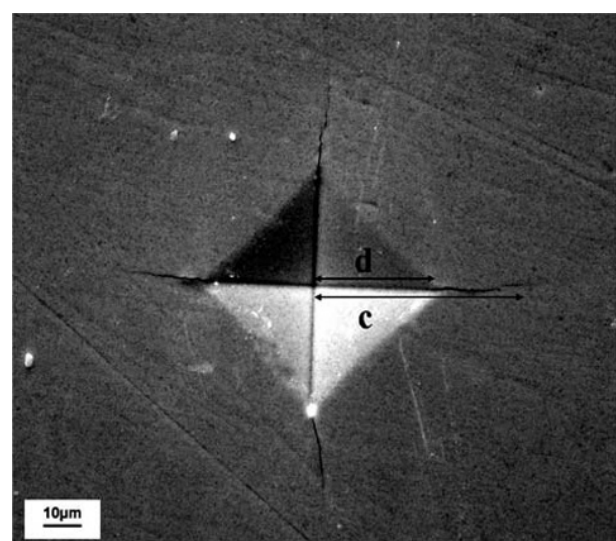


Fig. 4 : SEM image of an indentation on  $t'$  YSZ

around the crack. Larger tetragonality usually leads to higher ferroelastic toughening. Moreover, finer crystallite size may also lead to further increase the fracture toughness [19]. These considerations are commensurate with the observed high toughness behaviour in the present study. While it is difficult to retain nanocrystallinity at TBC application temperature, it may be beneficial to develop coatings with as small crystallite size as possible.

#### 4. Conclusions

The toughness of the densified  $\text{ZrO}_2\text{-}8 \text{ mol\% MO}_{1.5}$  ( $\text{M} = \text{Y}, \text{Yb}$  and  $\text{Gd}$ ) with the non-transformable  $\text{t}'$  phase has been measured. The metastable  $\text{t}'$  structure was confirmed by Raman spectroscopy. There was no role of stress induced transformation in  $\text{t}'$  YSZ which was confirmed by the Raman studies at crack tip. This remains to be ascertained in the case of  $\text{YbSZ}$  and  $\text{GdSZ}$ . Ferroelastic toughening is likely to be responsible for the high toughness values, apart from nanocrystalline crystallite sizes. The toughness behaviour indicates that rare-earth stabilisers can potentially lead to TBC compositions with sufficiently high toughness for long thermal cyclic life.

#### Acknowledgements

Financial support from the Department of Science and Technology, Govt. of India is gratefully acknowledged.

#### References

1. Padture N P, Gell M and Jordan E H, *Science*, **296** (2002) 280.
2. Evans A G, Mumm D R, Hutchinson J W, Meier G H and Pettit F S, *Progress in Material Science*, **46** (2001) 505.
3. Levi C G, *Current Opinion in Solid State and Material Science*, **8** (2004) 77.
4. Cao X Q, Vassen R and Stover D, *Journal of the European Ceramic Society*, **24** (2004) 1.
5. Clarke D R and Levi C G, *Ann. Rev. Mater. Res.*, **33** (2003) 383.
6. Miller R A, *J. Therm. Spray Technol.*, **6** (1997) 35.
7. Bratton R J and Lau S K, *Science and Technology of Zirconia*, Ed. Heuer A H, Hobbs L W, **3** (1984) 226.
8. Muraleedharan K, Subrahmanyam J and Badhuri S R, *J. Am. Ceram. Soc.*, **71** (1988) C226.
9. Miller R A, Smialek J L and Garlick R G, *Science and Technology of Zirconia*, Ed. Heuer A H, Hobbs L W, **3** (1984) 241.
10. Mercer C, Williams J R, Clarke D R and Evans A G, *Proc. Royal Soc. A*, **463** (2007) 1393.
11. Schaedler T A, Leckie R M, Kramer S, Evans A G and Levi C G, *J. Am. Ceram. Soc.*, **90** (2007) 3896.
12. Tolpygo V K and Clarke D R, *Acta Mater.*, **47** (1999) 3589.3605.
13. Mumm D R, Evans A G and Spitsberg I T, *Acta Mater.*, **49** (2001) 1029.
14. Choi S R, Hutchinson J W and Evans A G, *Mech. Mater.*, **31** (1999) 431.
15. Lange F F, *Mater. Sci.*, **17** (1982) 255.
16. Evans A G and Cannon R M, *Acta Metall.*, **34** (1986) 761.
17. Virkar A V and Matsumoto R L K, *J. Am. Ceram.*, **69** (1986) C-224.
18. Raghavan S, Wang H, Dinwiddie R B, Porter W D and Mayo M J, *Scripta Mater.*, **39** (1998) 1119-1125.
19. Anstis G R, Chantikul P, Lawn B R and Marshall D B, *J. Am. Ceram. Soc.*, **64** (1981) 533.
20. JCPDS Cards #48-0224
21. Yashima M, Ohtake K, Kakihana M, Arashi H and Yashimura M, *J. Phys. Chem. Solids*, **57**(1996) 17.
22. Lugh Vi and Clarke D R, *J. Am. Ceram. Soc.*, **88** (2005) 2552.
23. Shannon R D, *Acta Cryst.*, **A32** (1976) 751.
24. Lugh Vi and Clarke D R, *Surf. Coatings Tech.*, **200** (2005) 1287.
25. Barsoum M, *Fundamentals of Ceramics*, McGraw-Hill (1997) 415..